Open access • Journal Article • DOI:10.1016/J.CEP.2012.06.009

Fabrication and testing of a planar microstructured concept module with integrated palladium membranes — Source link

Tim Boeltken, M. Belimov, Peter Pfeifer, Thijs Peters ...+2 more authors

Institutions: Karlsruhe Institute of Technology, SINTEF

Published on: 01 May 2013 - Chemical Engineering and Processing (Elsevier)

Topics: Membrane, Concentration polarization, Microchannel and Permeation

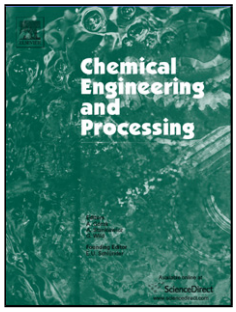

Title: Fabrication and testing of a planar microstructured concept module with integrated palladium membranes

Authors: T. Boeltken, M. Belimov, P. Pfeifer, T.A. Peters, R. Bredesen, R. Dittmeyer

PII: S0255-2701(12)00121-3
DOI: doi:10.1016/j.cep.2012.06.009
Reference: CEP 6143

To appear in: *Chemical Engineering and Processing*

Received date: 3-4-2012
Revised date: 22-6-2012
Accepted date: 24-6-2012

Please cite this article as: T. Boeltken, M. Belimov, P. Pfeifer, T.A. Peters, R. Bredesen, R. Dittmeyer, Fabrication and testing of a planar microstructured concept module with integrated palladium membranes, *Chemical Engineering and Processing* (2010), doi:10.1016/j.cep.2012.06.009

Fabrication and testing of a planar microstructured concept module with integrated palladium membranes

T. Boeltken[1]*, M. Belimov[1], P. Pfeifer[1], T.A. Peters[2], R. Bredesen[2] and R. Dittmeyer[1]

[1] Karlsruhe Institute of Technology (KIT), Institute for Micro Process Engineering (IMVT), Hermann-von-Helmholtz-Platz 1, 76344 Eggenstein-Leopoldshafen, Germany

[2] SINTEF Materials and Chemistry, P.O. Box 124 Blindern, N-0314, Oslo, Norway

* Corresponding author (tim.boeltken@kit.edu)

Highlights
Leak-tight integration of thin Pd-based membrane in a microstructured concept module
Extremely high selectivities for hydrogen separation
Minimization of concentration polarization effects
Calculation of film effectiveness factor

Abstract

A planar microstructured hydrogen separation module has been fabricated to study the hydrogen permeation through free-standing palladium-based membranes (Pd, PdCu and PdAg) with minimal influence by concentration polarization.

The membranes were laser-welded directly between two face-to-face arranged stainless-steel sheets with 10 microchannels each (width x depth x length of the channels: 500 µm x 300 µm x 2 cm).

Single gas hydrogen and mixed gas permeation experiments (H_2/N_2) were conducted between 300 and 400°C. The permeabilities and activation energies of the membranes in this temperature range were calculated.

The 12.5 µm thick membrane was successfully tested up to 650 kPa, indicating that the microchannel plates provide a good mechanical support even for very thin membranes. However, settling of the film into the microchannels on the permeate side was observed due to the overpressure on the retentate side suggesting even

finer channels and eventually the use of an additional porous support for very high differential pressure.

The concentration polarization effects in the membrane module were evaluated in terms of the film effectiveness factor η which is a familiar concept from heterogeneous catalysis. It could be shown that the microchannel configuration effectively decreases concentration polarization.

Introduction

The dominant route to produce hydrogen today is steam methane reforming, with typical capacities of up to 200.000 Nm³/h **[1]**. This is an endothermic equilibrium limited reactions and is represented together with the water-gas-shift reaction as follows:

$$CH_4 + 2\ H_2O \rightleftharpoons 4\ H_2 + CO_2 \qquad (1)\#$$

The reforming reaction is conducted over a Ni/Al_2O_3 catalyst at temperatures > 850°C and elevated pressures (1-4 MPa). The CO produced is converted with steam in a water-gas-shift reactor to generate additional hydrogen. The conversion of CO in the exothermic water-gas-shift reaction is also restricted by thermodynamics, which calls for more than one stage in order to reach a low CO content in the effluent. Final purification of the hydrogen is usually achieved by pressure swing adsorption.

Altogether, the separation of hydrogen from the gas mixture accounts for over 50% of the total plant costs **[2]**.

For small-scale industrial uses the distribution of hydrogen is mainly accomplished by truck delivery as cryogenic hydrogen or compressed hydrogen in gas cylinders.

In recent years, the industrial demand for pure hydrogen has been steadily growing, with notably many applications with rather small capacity for chemical processes. Moreover, production of hydrogen for fuel cell systems for clean power generation may become a new market of the future, as hydrogen is an important energy carrier in various future scenarios **[3]**.

An on-site production of hydrogen is favoured over a distribution system due to economical, ecological and safety reasons. However, downscaling of the conventional steam methane reforming process is not economically attractive, mainly

because the effort and the investment for the pressure swing adsorption unit is too high for smaller units **[4]**.

Membrane reformer systems for the processing of hydrocarbons have been frequently reported and discussed in the literature **[5, 6, 7]**. The main benefit from the integration of a palladium membrane in a steam reformer would be that the produced hydrogen is directly removed from the reaction zone at ultra-high purity while additional purification steps are not required **[8, 9]**. Furthermore, lower temperatures can be applied as the removal of hydrogen shifts the thermodynamic equilibrium **[10]**. Theoretical calculations show that satisfactory methane conversion can be achieved at 550°C, if 80% of the produced hydrogen is removed out of the reactor **[11]**.

Based on the open literature, today the membrane reactor with the technically most advanced level is a 40 Nm³/h-class membrane reformer system developed and run by Tokyo Gas Co., Ltd, with methane conversions of 80 – 95 % at an operating temperature of 495 – 540 °C **[12, 13]** and a carbon capture unit for reduced CO_2 emissions **[14]**.

The diffusion of hydrogen through a palladium membrane can be described as a multi-step mechanism from the high partial pressure side to the low partial pressure side: diffusion from the bulk gas to the surface of the membrane, adsorption of molecular hydrogen on the surface, dissociation and dissolution of the H in the bulk metal, diffusion of H through the bulk metal, release and recombination to hydrogen molecules, desorption on the low partial pressure side and diffusion from the membrane surface into the permeate gas **[15]**. Provided that the diffusion of atomic hydrogen through the bulk metal is the rate-determining step, the hydrogen flux through the membrane J_{H2} can be described by a combination of Fick's and Sieverts' law **[16]**:

$$j_{H_2} = \frac{Q}{s}\left(p_{H_2,R}^{n} - p_{H_2,P}^{n}\right) \qquad (2)$$

where Q is the permeability, s the thickness of the membrane and p_{H2} the partial pressure of the molecular hydrogen on the feed/retentate side (R) and on the permeate side (P), respectively. The permeability Q has an Arrhenius-type temperature dependency according to Eq. (3), with the pre-exponential factor Q_0, the activation energy E_a and the temperature T.

$$Q = Q_0 \varepsilon x p\left(-\frac{E_a}{RT}\right) \quad (3)$$

The quotient Q/s is called permeance π.

For the limitation of the hydrogen flux by bulk diffusion of H in the membrane n-values of 0.5 are often found (Sieverts' law), n values above 0.5 are attributed to an increasing influence of surface effects, usually for thinner membranes **[17, 18]**. More extensive models have been reported in literature which include adsorption and desorption effects in the overall hydrogen permeation process **[15, 19]**.

During the separation of hydrogen from a gas mixture several effects can occur, which decrease the hydrogen flux through the membrane:

1. Decrease of the hydrogen concentration due to the selective removal of hydrogen out of the gas mixture along the flow direction (hydrogen depletion).
2. In presence of adsorbable gases, such as carbon monoxide, available hydrogen dissociation sites may be blocked on the palladium surface leading to a decrease of the hydrogen flux (competitive adsorption) **[20, 21, 22]**.
3. Concentration polarization, i.e. reduction of the hydrogen concentration towards the membrane surface on the retentate side, or an increase of the hydrogen concentration towards the membrane surface on the permeate side, or both, caused by the existing gas phase mass transport resistances in the retentate and permeate side flow compartments or in a possible porous support **[23, 24, 25]**.

All three phenomena lead to a reduced driving force for permeation of hydrogen atoms through the metal layer. In particular for thin membranes exhibiting a high H_2 flux all three phenomena are important as the governing mechanism of hydrogen permeation may change from bulk diffusion control to surface or gas phase diffusion control **[15]**.

The effect of concentration polarization has been extensively studied by various research groups, mainly in tubular membrane configurations with distances between wall and membrane in the centimetre-range **[23, 24, 25]**. A negative influence on the hydrogen flux has been reported.

For this reason membrane configurations were developed where the distance between feed gas and membrane was decreased to the sub-millimetre region leading to thin laminar layers and high flow velocities to increase the mass transfer rate and

reduce concentration polarization: Mori et al. **[24]** reported an increased methane conversion and hydrogen recovery while decreasing the diameter of the tubular reactor (from 40 to 16 mm) and decreasing the distance between the wall of the outer tube and the inner membrane (from 15 to 3 mm).

Ryi et al. **[26]** and Hwang et al. **[27]** reported a circular composite membrane integrated in a housing. Hydrogen permeation experiments were conducted with 40 vol.% CO_2 in H_2. The distance between the wall of the housing on the feed side and the membrane surface was reduced from 2.5 mm to 0.4 mm which gave rise to an increase of the H_2 recovery by 25% at 1600 kPa and a feed flow rate of 2000 ml/min.

Mejdell et al. reported microchannel configurations with channel diameters of 1 mm and 0.2 mm **[17, 22]**. The microchannel configuration showed promising results to enhance the hydrogen flux through the membrane by decreasing concentration polarization effects **[17]**.

In this paper we present a microchannel membrane module equipped with palladium membranes of various thicknesses. The microchannels serve as mechanical support for the membrane sheets.

Membrane integration is a crucial factor for the construction of membrane modules for technical applications. The module with composite membrane of Ryi et al. **[26]** and Hwang et al. **[27]** was fastened with bolts and sealed with two O-rings**.**

Mejdell et al. **[17, 21, 22]** clamped the membrane between the feed and the permeate housings. Sealing was achieved by pressing the membrane between the highly-polished faces of the housings.

The membranes in our microstructured concept module were leak-tight integrated between thin metal sheets by laser-welding. This considered a very practical approach and represents a first step towards a compact multi-layered microchannel membrane reformer system. Since concentration polarization effects are expected to be subordinate, a high space-time-yield is anticipated due to the supplied high volumetric surface area for reaction and membrane separation. Moreover, the outstanding heat transfer performance of microchannel systems should enable high energy efficiency **[28]**.

Experimental

Microstructured membrane module preparation

A microstructured concept membrane module has been designed to study the integration of the metallic membrane between microstructured foils and its performance.

The module consists of a cover and a bottom plate (material stainless steel: 1.4408). Both plates each contain 10 microchannels with a width, depth and length of 500 µm x 300 µm x 2 cm, resulting in an effective membrane area of 1 cm². Holes were milled through the plate at the end of each channel acting as inlet and outlet for feed and retentate flow on the top side and for sweep gas and permeate flow on the bottom side of the module.

The microstructured sheets where arranged face-to-face with a palladium-based membrane placed between the two sheets (Fig. 1). Four different membranes were used in the experiments.

A cold-rolled PdCu membrane with a nominal thickness of 50 µm was supplied by MaTeck. A cold-rolled 12.5 µm thick Pd membrane was obtained from Goodfellow Special Metals. These two membranes were cut down to the size of the microstructured module.

In addition, a 13 µm and a 4.7 µm thick PdAg membrane were supplied by SINTEF. These two membranes were prepared by magnetron sputtering on silicon wafer substrates **[29]**. Before mounting them between the microstructured plates they were cut on the silicon wafer into the adequate size and peeled off.

The arrangements consisting of a membrane and the microstructured sheets were laser-welded from the top, i.e., by welding through the stacked plates, see Fig. 2. A cavity on the top plate prevented protrusion of the weld seam and allowed its aligning with the surface of the membrane module. The microstructured modules were integrated into the housing with connections for the gas supply, see Fig. 3.

Figure 1 here

Figure 2 here

Figure 3 here

The inlets and outlets on the backside of the microchannel plates were connected to the housing with graphite seals. The total arrangement is called membrane device. A schematic of the microstructured membrane module is shown in Fig. 4.

Figure 4 here

Membrane characterization

The surface morphology of the four different membranes as well as the cross-sections of the modules with the integrated membranes where characterized with SEM and WDX with a JEOL JXA-8530F field emission electron probe microanalyzer (EPMA). The actual membrane thickness was determined with SEM after the integration of the membrane in the microstructured membrane module and after hydrogen permeation experiments.

Hydrogen Permeation Measurements

Hydrogen and nitrogen were fed to the membrane module with mass flow controllers (Bronkhorst EL-FLOW®). Permeate and retentate flow rates were measured using a soap bubble flow meter.

In addition, the composition of the retentate and permeate were frequently analyzed using a gas chromatograph (Agilent 6890A) equipped with FID and TCD as well as a PoraPlot and a molsieve 5Å capillary column (Agilent). In cases where the permeate flow was not high enough for GC measurements a make-up gas was admixed behind the membrane module.

The housing was electrically heated with three heating cartridges on each side. The feed and the optional sweep gas were preheated to the temperature of the membrane device.

At the beginning of the experiments, the membrane device was ramped to the desired temperature (1°C/min) while flushing with nitrogen on the feed side as well as on the permeate side. At the target temperature the flow of nitrogen on the permeate side was stopped and the ideal permselectivity of the membrane was measured: For this the membrane was pressurized with pure nitrogen on the feed side, and the flow of nitrogen through the membrane was measured. Then, the nitrogen feed flow was

decreased to zero while hydrogen was slowly introduced into the feed and the H_2 flux was left for equilibration for the next 24 hours. The volume flow of hydrogen through the membrane at the same temperature and pressure was used to calculate the ideal permselectivity of the membrane according to Eq. (5):

$$S = \left.\frac{\dot{V}_{H_2}}{\dot{V}_{N_2}}\right|_{p,T} \quad (5)$$

The retentate pressure was regulated using a needle valve and a digital pressure meter (Greisinger electronic GMH 3150), while the permeate side was kept at atmospheric pressure at all times.

For the determination of the activation energy of hydrogen permeation, only hydrogen at a relatively high volume flow (250 ml/min) was introduced on the feed side while no sweep was applied on the permeate side to ensure well-defined hydrogen partial pressures on both sides of the membrane. Before each experiment at a certain pressure and temperature, the membrane was equilibrated for 24 hours at the maximum pressure and temperature of the parameter field (different for the individual membranes due to different material and thickness).

With this procedure an irreversible deformation of the membrane in the microchannels was enforced to avoid possible undesired effects associated with membrane surface enlargement during the experiments which could lead to hysteresis **[30]**.

Hydrogen Separation Measurements

Given the case that hydrogen is present on the feed side in a gas mixture, a limitation of the flux by diffusion of hydrogen from the channel to the membrane surface often referred to as 'concentration polarization' must be considered. The situation may be represented by the concept of a laminar boundary layer introducing the mass transfer coefficient k_G to describe the diffusion resistance (Fig. 5).

Figure 5 here

In Fig. 5 $p_{H2,R}$ represents the H_2 partial pressure on the feed/retentate side, $p_{H2,P}$ the H_2 partial pressure on the permeate side and p_{H2}* the H_2 partial pressure directly at

the membrane surface. The hydrogen flux through the boundary layer $j_{H2,F}$ can be expressed based on Fick's law (Eq. 6):

$$j_{H_2,F} = \frac{k_G}{RT}\left(p_{H_2,R} - p_R^*\right) \quad (6)$$

whereas Sieverts' law is invoked to represent the hydrogen flux through the membrane:

$$j_{H_2,M} = \pi\left(p_{H_2}^{*0.5} - p_{H_2,P}^{0.5}\right) \quad (7)$$

In steady state the H_2 flux through the boundary layer must equal the H_2 flux through the membrane, so by equating $j_{H2,F}$ and $j_{H2,M}$ and rearranging the unknown H_2 partial pressure at the membrane surface p_{H2}^* can be expressed in terms of the known partial pressures on the feed/retentate and permeate side (Eq. 8).

$$p_{H_2}^* = p_{H_2,R} + \frac{p_{H_2,P}^{0.5}}{f} + \frac{1}{2f^2} - \frac{1}{f}\sqrt{p_{H_2,R} + \frac{p_{H_2,P}^{0.5}}{f} + \frac{1}{4f^2}} \quad (8)$$

Where $f = \frac{k_G}{RT}\frac{1}{\pi}$ measures the ratio of the mass transfer coefficient of the boundary layer and the membrane permeance.

The 'ideal' H_2 flux through the membrane, i.e., in absence of any concentration polarization, is obtained by invoking Sieverts' law with the hypothetical (i.e., 'highest possible') driving force $\left(p_{H_2,R}^{0.5} - p_{H_2,P}^{0.5}\right)$ (Eq. 2). By relating the actual flux $j_{H2,F}$ to the ideal flux, e.g., division of Eq. (6) by Eq. (2), a film effectiveness factor η can be defined:

$$\eta = \frac{j_{H_2,F}}{j_{H_2}} = \frac{\left(p_{H_2,R} - p_{H_2,R}^*\right)}{\left(p_{H_2,R}^{0.5} - p_{H_2,P}^{0.5}\right)} \quad (9)$$

Substituting Eq. (8) into Eq. (9) and rearranging finally gives an equation for determining the film effectiveness factor as a function of the parameter *f* and the known H_2 partial pressures in the feed/retentate and permeate.

$$\eta = \frac{\sqrt{1+2\rho\phi+\phi^2}-\phi-\rho}{1-\rho} \quad (10)$$

where ρ and Φ are two dimensionless numbers, defined by Eqs. (11) and (12), respectively.

$$\Phi = \frac{1}{2f\sqrt{\beta_{H_2,R}}} \tag{11}$$

$$\rho = \sqrt{\frac{p_{H_2,P}}{p_{H_2,R}}} \tag{12}$$

A double logarithmic plot of η from Eq. (10) versus Φ is shown in Fig. 6 for different values of ρ as a parameter. The shape of the curves corresponds to effectiveness factor plots known from heterogeneous catalysis. The effectiveness factor tends to approach 1 for small values of Φ whereas the asymptotic solution for large values of Φ is η ~ 1/ Φ. From the definition of Φ together with Fig. 6, it is obvious that a higher H_2 partial pressure on the retentate side at unchanged H_2 partial pressure on the permeate side leads to an increased effectiveness factor. This is due to the linear partial pressure dependence of the H_2 flux through the boundary layer (Eq. 6) as opposed to the (weaker) square root dependence for the membrane (Eq. 7). Moreover, we note from Fig. 6 that a lower value of ρ leads to a lower effectiveness factor. The parameter ρ is an indication of the driving force for H_2 permeation. Yet the conclusion is not that a higher driving force generally would lead to a lower effectiveness factor. Instead, the point is that the effectiveness factor gets reduced when the driving force is increased by lowering the H_2 partial pressure on the permeate side. In that case, for unchanged $p_{H2,R}$, Φ is constant, and we move from a starting point in Fig. 6 vertically down towards a lower value of ρ. On the contrary, if the driving force is increased by raising the H_2 partial pressure on the retentate side, we generally move on a diagonal line in Fig. 6 because in addition to the decrease of ρ we will simultaneously decrease the value of Φ.

Figure 6 here

The benefit of Fig. 6 or Eq. (10) is that the influence of the retentate side mass transfer on the effective hydrogen flux can be determined once the true hydrogen permeance of the membrane is known and the mass transfer coefficient on the retentate side can be estimated.

It may be obvious to note here that a similar approach could be applied to take into account the influence of a porous support on the retentate side as well as the influence of a possible mass transfer limitation on the permeate side if a sweep gas is used for enhancing the H_2 flux. Yet this has not been the case for our measurements.

To further analyse our permeation data, we introduce a hydrogen recovery factor φ_{H2}:

$$\varphi_{H_2} = \frac{\dot{V}_F}{\dot{V}_F}\left(x_{H_2,F}\frac{p_F}{p_F} - \frac{\left(1-x_{H_2,F}\right)}{\left(1-\frac{p_F}{p_F}\right)}\right)^{-1} \tag{13}$$

which takes into account that hydrogen removal through the membrane will stop once the hydrogen partial pressures on both sides of the membrane equilibrate. In Eq. 13 the hydrogen recovery factor φ_{H2} becomes 0 if no hydrogen at all is separated and 1 if the maximum amount of hydrogen is removed, i.e., the partial pressures of hydrogen in the permeate and retentate side equilibrate.

Due to hydrogen removal along the membrane, the H_2 partial pressure on the retentate side will change along the membrane. In turn Eqs. (6) - (12) have to be invoked locally, i.e., for any position along the membrane. As a consequence, the hydrogen flux and the film effectiveness factor may change along the membrane. This was considered for the evaluation of concentration polarization effects during our measurements in the membrane module shown in Fig. 4, by using a one-dimensional simulation model coded in Matab® with the above equations implemented. The mass transfer coefficient k_G was obtained according to film theory as quotient of the diffusion coefficient D_{H2N2} and the thickness of the boundary layer d_{lam} (Eq. 14).

$$k_G = \frac{D_{H_2N_2}}{d_{lam}} \tag{14}$$

The boundary layer thickness d_{lam} was taken as the height of the microchannels and the weak influence of the mean flow velocity on k_G, expected for microchannel flows, was neglected.

In addition to the 'local' film effectiveness factor given by Eq. (10), the simulation model was also used to derive a 'global' effectiveness factor η_{glob} which is defined according to Eq. (15) as the ratio of the absolute molar flow rate of permeated

hydrogen under actual conditions to the absolute molar flow rate of the permeate in absence of any gas phase mass transfer limitations ($k_G \to \infty$).

$$\eta_{glob} = \frac{\dot{n}_{H_2,P}}{\dot{n}_{H_2,P,ideal}} \quad (15)$$

Results and discussion

Membrane characterization and integration

Fig. 7 shows the SEM images of the (feed) surface of the four fresh membranes. The different preparation techniques have an impact on the surface structure of the membrane.

The PdCu membrane was prepared by cold-rolling. The imprint of the rollers clearly indicates the direction of graining/rolling.

The Pd membrane was cold-rolled down to 12.5 µm and ordered with light-tight specification. For the preparation of membranes with this specification cold-rolling has to be done under cleanroom conditions and using very smooth rolls. The SEM picture shows that the direction of graining is not identifiable. The surface structure of the 12.5 µm Pd membrane might originate from the roughness of the rolls, as the same microstructure was identified on both sides of the membrane.

The surfaces of the SINTEF membranes show a different topology depending on the side of the membrane. A characteristic pattern for a sputtered surface is identified for the original growth surface of the membrane. The surface in contact with the silicon wafer during sputtering shows a perfect uniformity (too smooth to be imaged) **[31]**. The grain size of the sputtered surface increases with increasing membrane thickness **[32]**. The growth surface formed during magnetron sputtering was placed in the microstructured module facing the feed gas flow (high pressure side), while the smooth surface was facing the permeate side (low pressure side) **[31, 32]**.

Figure 7a here

Figure 7b here

Figure 7c here

Figure 7d here

The fresh surface of the palladium-alloy membranes was further characterized with WDX analysis for the determination of the composition of the membranes (see Table 1). Measurements were made at three different positions on the surface.
The PdCu membrane is composed of 47 at.% Pd and 53 at.% Cu, which corresponds to around 60 wt.% Pd and 40 wt.% Cu. The PdAg membranes showed a composition of 80 at.% Pd and 20 at.% Ag.
The cross-sections of the microstructured modules with the PdCu and both PdAg membranes are shown in Fig. 8. They were prepared after the permeation experiments, i.e., after pressurizing the membranes. Fig. 8a) and 8b) show the arrangement of the membrane after plastic deformation during permeation experiments. The small gap in Fig. 8c) originates from the embedding of the cut module in the resin for preparation of the cross section and does not represent the membrane situation during permeation experiments.

Figure 8a here

Figure 8b here

Figure 8c here

Bending of the thin membranes (4.7 µm, 12.5 µm and 13 µm) in the microstructures on the permeate side was observed. This may result in an enlargement of the membrane surface and a reduction of the membrane thickness.
As it was not part of this work to analyse the effect of surface enlargement and accessibility of the Pd membrane on the fins of the microstructure, the effective surface area for hydrogen separation was taken as the free membrane surface between the fins of the microchannels (1 cm^2). This may, however, lead to an underestimation of the actual membrane surface and thus to an overestimation of the hydrogen flux and permeability of the thin membranes (4.7 – 13 µm).
The stacking arrangement of the microstructures against each other worked quite well in all modules except for the 13 µm PdAg membrane (Fig. 8b). This

misalignment may be associated with an increased surface area for hydrogen permeation, but additionally also with an asymmetric hydrogen concentration profile in the PdAg membrane.

It is important to note that the effective membrane surface for hydrogen dissociation in the microstructured module is not precisely known. The membrane surface of the feed side, for example, might have been completely accessible for hydrogen dissociation after pressurization of the membrane module.

Furthermore, it is assumed that the cross-sections of the membrane modules were embedded precisely at right angle in the sample holder for EPMA analysis and determination of the thicknesses of the membranes from the SEM pictures in Fig. 8. The thickness of each membrane was averaged over the entire cross section (free area and clamped area between the fins) and shown in Table 1.

Hydrogen permeation results

Several pure and mixed gas experiments were conducted to evaluate the performance of the laser-welded microstructured membrane modules. The initial values of the ideal permselectivity for the different membrane modules are shown in Table 1 together with the elemental compositions and thicknesses of the membranes and the experimental conditions.

Table 1 here

After integration of the membranes in the microstructured module, the measured ideal permselectivity is not only an indication for the integrity of the membrane, but also of the quality of the weld seam. This is particularly evident when comparing the selectivity of the 61 µm thick PdCu to that of the 12.5 µm thick Pd membrane. Although the PdCu membrane is 5 times thicker than the Pd membrane, and hence the probability for defects allowing some N_2 to leak through should be lower, its selectivity is around 15 times lower. Even though defects in the PdCu membrane originating from the cold-rolling process cannot be ruled out completely, it seems more likely that some leaks were formed where the metallic microchannel foils and the metallic membrane were joined by laser welding.

All measured ideal permselectivities are very high, which confirms the good quality of the membranes used as well as for the good quality of the weld seam.

Pure hydrogen permeation

Permeation experiments with pure hydrogen on the feed side were conducted to determine permeance, permeability and activation energy for each membrane. No sweep gas was used, and the pressure at the permeate side was kept at atmospheric level at all times.

In Fig. 9 the hydrogen flux obtained at 350°C is plotted over the difference of the square root of the partial pressures of hydrogen (Sieverts plot) for all four membranes tested. The hydrogen flux as a function of the hydrogen partial pressure difference is well described with the hydrogen partial pressure exponent of 0.5 (Sieverts' law), see Eq. (2). This indicates that the hydrogen transport is mainly controlled by bulk diffusion of hydrogen atoms through the dense membrane **[18]**.

Permeance and permeability values for pure hydrogen experiments were calculated by linear regression based on the experimental data at each temperature, shown as dotted lines in Fig. 9.

Figure 9 here

The hydrogen flux through the membrane increases as expected with increasing trans-membrane hydrogen partial pressure difference and decreasing membrane thickness, according to Eq. (2). For example, the H_2 flux through the 4.7 µm PdAg membrane was 0.40 mol/(m²s) at a feed pressure of 150 kPa and 1.26 mol/(m²s) at a feed pressure of 300 kPa. The H_2 flux through the 61 µm PdCu membrane the flux was 0.15 mol/(m²s) at a feed pressure of 650 kPa.

The H_2 flux of the 13 µm PdAg membrane at 450 kPa is nearly twice as high as the H_2 flux of the 12.5 µm Pd membrane at 350°C, albeit their similar thickness. This is explained by the fact that alloying Pd with Ag leads to an expansion of the lattice constant of the metal **[33]**, which accelerates the hydrogen permeation through the bulk metal **[34]** and increases the solubility of H_2 in the PdAg alloy compared to pure Pd **[35]**.

The temperature dependence of the permeance of each membrane is shown in Fig. 10. It seems that the Arrhenius law can be applied to the experimental data. From the linear fit of the experimental values the apparent activation energies for the Pd and PdAg membranes are in the range of 10.4 kJ/mol to 14.6 kJ/mol. The apparent activation energy for the PdCu membrane is 6.5 kJ/mol.

Figure 10 here

The obtained permeabilities and activation energies of the four membranes are compared to some published data in Table 2.

Table 2 here

It is obvious that the comparison of results with published data in literature is difficult due to the wide range of temperatures and pressures utilized for permeation experiments, the different membrane compositions and support materials used and the inconsistent units employed in the calculation of the permeability. The microstructure of the membrane and surface impurities may also have an effect on the permeability derived **[35]**.

In addition, the thickness of membranes deposited on porous supports is often difficult to determine precisely.

On the one hand, the obtained permeabilities in this work are all within the range of 10^{-8} mol/(ms$Pa^{0.5}$) and in good comparison with the permeabilities for unsupported Pd-based membranes were bulk diffusion limitation seems likely (e.g. **[16, 42, 47]**). This indicates, that the assumption of an effective membrane area of 1 cm² (free membrane surface) seems legitimate.

On the other hand, much lower permeabilities have been obtained by a number of researchers. This may be due to the influence of a porous support which first of all leads to a reduction of the accessible membrane area at the interface between the membrane and the support. Moreover a porous support may also lead to a reduced H_2 partial pressure at the membrane surface compared to the free gas phase if placed on the feed side, or to an increased H_2 partial pressure at the membrane surface if placed on the permeate side. Additionally, the application of sweep gas on the permeate side of the membrane may lead to a transition from the bulk diffusion

limited region to a desorption-limited region under certain circumstances **[15]**. Moreover, if sweep gas is used concentration polarization effects may occur on the permeate side as well. This is of special importance, when supported membranes are used with the support placed on the permeate side.

However, we did not apply sweep gas during our permeation experiments. Therefore our data are free of these effects.

Permeability values for similar PdAg membranes are reported in literature: At 300°C Mejdell et al. **[31]** obtained a permeability of around 1.5 x 10^{-8} mol/(ms$Pa^{0.5}$) for a ~ 5 µm thick PdAg membrane, while Tucho et al. **[32]** obtained a permeability around 2.8 x 10^{-8} mol/(ms$Pa^{0.5}$) for a ~ 6 µm thick PdAg membrane. This shows that variations are found from batch to batch for sputtered membranes. We obtained a permeability of 2.2 x 10^{-8} mol/(ms$Pa^{0.5}$) for the 4.7 µm thick PdAg membrane which fits well into the range of reported values.

Tucho et al. **[32]** additionally obtained permeabilities ranging from of 2.1 x 10^{-8} – 3.1 x 10^{-8} mol/(ms$Pa^{0.5}$) for a ~ 10 µm thick PdAg membrane at 300°C. The permeability of the 13 µm thick PdAg membrane used in this work at 300°C is 3.0 x 10^{-8} mol/(ms$Pa^{0.5}$), which is high, but still in the range reported by Tucho et al. **[32]**. As pointed out above some uncertainty remains in our data for the 13 µm thick PdAg membrane concerning the effective membrane area due to the misalignment of the two microchannel foils, see Fig. 8.

The obtained activation energies for the four different membranes are within the range reported in literature as well, but there again a large scattering of the reported values is to be noted.

On the one hand, apparent activation energies between 5 and 10 kJ/mol are considered for bulk diffusion limitation **[18]**. On the other hand, much higher (> 40 kJ/mol) and also lower values for the activation energy have been reported, which suggests further investigations on the influence of processes on the membrane surface on the overall performance.

In general, activation energies of around 14 kJ/mol are expected for bulk diffusion limitation **[16]**, which is close to the values derived in this work (Table 2).

The results indicate that even for the thinnest PdAg membrane of 4.7 µm the hydrogen transport is mainly determined by bulk diffusion through the membrane.

Deviation from bulk diffusion limitation often occurs for thin membranes, which are influenced by surface effects, leakage through defects of the membrane, transport

resistance of the substrate material, palladium surface contamination, palladium support-interface effects, flow of hydrogen across grain boundaries, thermal hysteresis, lattice dilatation or lattice defects **[16]**.

Therefore, in literature the n-value is often fitted to the experimental results. An n-value deviating from 0.5 is then explained with increasing influence of surface processes on the hydrogen transport **[16, 18, 26, 30]**.

A least-square regression technique was implemented to determine the best fit of the experimental data for each membrane. The n values were 0.56 for the 61 µm thick PdCu membrane, 0.62 for the 12.5 µm thick Pd membrane, 0.63 and 0.81 for the 13 µm and 4.7 µm thick PdAg membranes, respectively. The deviation of the fitted n-value from the Sieverts exponent 0.5 increases with decreasing membrane thickness.

This could be taken as an indication that surface processes have a greater influence on the hydrogen permeation process for the thinner membranes **[15].**

McLeod et al. summarized the limitations of the fitting of the pressure exponent to experimental data **[18]**. Often experiments are not conducted over a wide range of partial pressure, defects may artificially inflate the n-value due to viscous flow and Knudsen diffusion, and finally, the Sieverts' law is only valid over a specific range of temperature and pressure, resulting in a deviation of the n-value of 0.5 even if bulk diffusion limits the hydrogen permeation rate.

Taking the activation energy values reported in this work into account, we conclude that even for the thinnest PdAg membrane of 4.7 µm the hydrogen transport is mainly determined by bulk diffusion of H atoms through the membrane.

As the n-value of 0.5 represents a very good fit of our data (see Fig. 9) this value was chosen as the basis for all our plots and calculations.

Mixed gas permeation

Mixed gas experiments with H_2/N_2 mixtures were conducted with the 12.5 µm thick Pd membrane and the 4.7 µm thick PdAg membrane. For determination of the influence of concentration polarization effects, different feed flow rates were applied. In Fig. 11 the obtained H_2 flux of a 50 vol.% H_2/50 vol.% N_2 mixture at a retentate pressure of 300 kPa is shown as a function of total feed flow. The H_2 flux through the 4.7 µm PdAg membrane is higher than the H_2 flux through the 12.5 µm Pd

membrane due to the higher permeance of the PdAg membrane. With decreasing total feed flow rate the H_2 flux through the membrane decreases as driving force for hydrogen permeation.

Figure 11 here

The comparison of measured and simulated H_2 fluxes in Fig. 11 shows that the approach taken here to describe the influence of the retentate-side gas phase mass transfer resistance on the hydrogen separation performance of the module seems valid. Note that no fitting parameters were involved. The H_2 permeance was taken from the single gas data while the gas phase mass transfer was described by the mass transfer coefficient determined from Eq. (14). The simulation results agree well with the experimental values except for two points obtained with the 4.7 µm thick PdAg membrane at low feed flow rates (100 and 60 ml/min). The error bars for the experimental values in Fig. 11 result from the statistical variation of a number of replicate measurements with the soap bubble flow meter plus an anticipated eventual systematic error which was estimated from measurement uncertainty. For the two experimental data which are clearly off the corresponding simulation results, the experimentally determined H_2 recovery factors (Eq. 13) do exceed the maximum possible value of 1, i.e., φ_{H2} was 1 for 100 ml/min and 1.2 for 60 ml/min feed flow rate. This indicates a problem with these two measurements which may be explained by some deviation of the H_2 mole fraction in the feed flow from the setpoint.

The global film effectiveness factor η_{glob} (Eq. 15) and the calculated H_2 recovery factor φ_{H2} (Eq. 14) are shown as a function of the feed flow rate in Fig. 12. The recovery factor increases with decreasing total feed flow rate for both membranes, as expected. The calculations for the 4.7 µm PdAg membrane predict about 87% H_2 removal for a feed flow rate of 100 ml/min and 97% for a feed flow rate of 60 ml/min. As stated, the experimental data suggested here that more hydrogen was removed than expected for identical H_2 partial pressures on either side of the membrane in the permeate and retentate effluents. At low feed flow rates larger relative errors are generally expected as represented also by the error bars in Fig. 11. However, a change of the membrane during the measurements cannot be excluded which may have resulted in an increased permeation flow. It should be noted, however, that N_2 was never detectable in the permeate effluent by GC measurements during all

hydrogen separation measurements. Unfortunately, the membrane ruptured during replicate measurements with pure nitrogen meant to confirm the ideal permselectivity, so the mixture permeation experiments for 100 ml/min and 60 ml/min total feed flow rate could not be repeated. In conclusion, these two data points are treated as outliers.

Figure 12 here

With values between 87% and 97% we note that the global film effectiveness factor η_{glob} is generally high for the 12.5 µm Pd membrane as well as for the 4.7 µm PdAg membrane, i.e., the enrichment of the inert gas and concomitant depletion of hydrogen towards the membrane surface in the microchannels seems moderate. With decreasing membrane thickness the hydrogen flux increases due to the inversely proportional relationship (Eq. 2). Therefore, lower η values were found for the 4.7 µm PdAg membrane at feed flow rates between 200 and 400 ml/min compared to the 12.5 µm Pd membrane.

The trend for η_{glob} in Fig. 12 obviously is to increase with decreasing feed flow rate. Yet this is not expected based on the above derived equations, because at reduced flow velocity the mass transfer coefficient will not be higher and the steeper decline of the H_2 partial pressure along the membrane is expected to reduce the local film effectiveness factor, as has been explained in the context of Fig. 6. This is also seen in Figs. 13 and 14 showing the local H_2 fluxes from Eqs. (2) and (6) as well as the local film effectiveness factor according to Eq. (9) along the membrane for two sets of experimental conditions referring to measurements performed with the 4.7 µm PdAg membrane. Note that, on average, the local film effectiveness factor is slightly lower for the experiment at low flow rate, but the difference is truly small.

Figure 13 here

Figure 14 here

On the contrary, the global effectiveness factors derived from Eq. (15) differ significantly for the two experiments, i.e., ca. 87% for 400 ml/min and 98% for 60

ml/min. The point to be made here is that the global effectiveness factor is not only influenced by the gas phase mass transfer resistance, which reduces the effective local driving force over the membrane, but also by the decrease of the flux along the membrane due to the declining driving force in direction of the flow. In other words, although at low flow rate the mass transfer limitation gets even slightly worse due to the two effects outlined above, the available membrane area is still high enough to separate a higher fraction of the total hydrogen amount supplied with the feed, just because the feed flow rate per unit area of the membrane is much lower. Only for the limiting case of a hydrogen removal factor approaching zero, Eqs. (9) and (15) will give the same results. The higher the H_2 removal factor, the more pronounced the difference will be. In cases when the H_2 removal approaches 1, the performance of the module is no longer controlled by the kinetics but by the thermodynamics. Under such conditions no conclusion at all can be drawn about possible mass transfer limitations.

Hence, the global effectiveness factor in general is not a reliable measure of mass transfer limitations inside a membrane module. The same conclusion holds for the concentration polarization coefficient CPC which is basically identical to 1 – η **[25]**.

Experimentally, only the global entities are accessible, be it the film effectiveness factor or the concentration polarization coefficient. This brings about the risk of misinterpretations if conditions are applied at which the H_2 removal factor is high. Note that this is completely analogous to investigations on the kinetics of chemical reactions. There, reactant conversions too close to the equilibrium have to be avoided to guarantee that the results are controlled by the kinetics and not by the thermodynamics.

Practically, for a Pd-based membrane in a technical system, the entire membrane area should be utilized as good as possible. Therefore, a suitable compromise must be found balancing the conflicting goals of high hydrogen recovery factor and high hydrogen flux on the module level. In general, a high hydrogen recovery factor will be given the preference, e.g., 90%, while striving for high local film effectiveness factors.

In that sense the results obtained with the microstructured concept membrane module are very promising. Although the local film effectiveness factors still stayed below 1, they seem to be significantly higher than in larger flow geometries.

Summary and conclusions

Microstructured modules with leak-tight integrated palladium-based membranes of different thicknesses have been fabricated.

A PdCu membrane (thickness 61 µm), a Pd membrane (12.5 µm) and two PdAg membranes (13 and 4.7 µm) were used and an almost leak-free integration of the membranes was achieved by laser-welding. The leak-tightness was demonstrated by resulting H_2/N_2 ideal permselectivities between 1900 and > 30000.

A set of permeation tests with pure hydrogen and mixed gas compositions (H_2/N_2) were conducted to study the effect of concentration polarization on the permeation rate of the membrane. Hydrogen permeation experiments provided data which agreed with the literature for permeance and activation energy for free-standing Pd-based membranes without an additional porous support in the temperature range of 350 - 400°C for the PdCu and Pd membrane and 300 - 350°C for the PdAg membranes.

Membrane stability was achieved at least up to 650 kPa for the 61 and 12.5 µm thick membranes, 450 kPa for the 13 µm thick PdAg membrane and 300 kPa for the 4.7 µm thick PdAg membrane. The maximum bursting pressure was never reached during the experiments. This shows that the microstructure serves as a good support for the palladium membranes.

The gas phase mass transfer resistance inside the microstructured membrane module was analysed, and it could be shown that the microchannel configuration effectively suppresses concentration polarization effects and therefore enables high film effectiveness factors. Moreover, it could be demonstrated that local effectiveness factors which are accessible through simplified models are more reliable measures of possible gas phase mass transfer limitations than the global values derived on the module level. Experiments for analysis of concentration polarization effects must be performed in the kinetic regime, i.e., when the H_2 partial pressures in the retentate and permeate effluents are far from equilibration.

The design presented here is seen as a first step towards a compact microstructured membrane reformer, where the microstructure of the feed side is coated with a catalyst layer for reforming reactions. Further modification of this design is necessary for the application of the planar microstructured modules at reforming conditions. For example a porous diffusion barrier must be applied on the fins, which prevents

diffusion of metal atoms from the module into the Pd-based membrane and vice versa. It may also turn out that an additional mechanical support is needed at higher pressures. Technically, the size of the membrane sheets will have to be enlarged and a stack composed of many sheets will have to be assembled in order to provide a sufficiently large membrane area per volume.

The superior mass transfer properties of shallow microchannels in combination with thin Pd-based membranes were demonstrated. Due to the high local film effectiveness factors together with the further expected benefits of a microstructured reactor (compact construction, optimised heat supply to the catalyst and high space-time yield) a microstructured membrane reformer is regarded to exhibit higher efficiency for on-site production of pure hydrogen than conventional reformers.

Acknowledgements

We would like to thank Mrs. Uta Gerhards and Mr. Florian Messerschmidt, IMVT, for EPMA investigations. The financial support of the Helmholtz Research School for Energy-Related Catalysis is gratefully acknowledged.

References

[1] J.R. Rostrup-Nielsen, Fuels and Energy for the Future: The Role of Catalysis, Catal. Rev. – Sci. Eng. 46 (2004) 247-270.

[2] J.A. Ritter, A.D. Ebner, State-of-the-Art Adsorption and Membrane Separation Processes for Hydrogen Production in the Chemical and Petrochemical Industries, Sep. Sci. Technol. 42 (2007) 1123-1193.

[3] P. Moriarty, D. Honnery, Hydrogen's role in an uncertain energy future, Int. J. Hydrogen Energy 34 (2009) 31 – 39.

[4] N.W. Ockwig, T.M. Nenoff, Membranes for Hydrogen Separation, Chem. Rev. 107 (2007) 4078-4110.

[5] S. Uemiya, Brief review of steam reforming using a metal membrane reactor, Top. Catal. 29 (2004) 79-84.

[6] F. Gallucci, A. Basile, A. Iulianelli, H.J.A.M. Kuipers, A Review on Patents for Hydrogen Production Using Membrane Reactors, Recent Patents on Chemical Engineering 2 (2009) 207-222.

[7] B.N. Lukyanov, D.V. Andreev, V.N. Parmon, Catalytic reactors with hydrogen membrane separation, Chem. Eng. J. 154 (2009) 258-266.

[8] M. Oertel, J. Schmitz, W. Weirich, D. Jendryssek-Neumann, R. Schulten, Steam Reforming of Natural Gas with Integrated Hydrogen Separation for Hydrogen Production, Chem. Eng. Technol. 10 (1987) 248-255.

[9] J. Tong, Y. Matsumura, H. Suda, K. Haraya, Experimental Study of Steam Reforming of Methane in a Thin (6μM) Pd-Based Membrane Reactor, Ind. Eng. Chem. Res. 44 (2005) 1454-1465.

[10] F. Gallucci, A. Comite, G. Capannelli, A. Basile, Steam Reforming of Methane in a Membrane Reactor: An Industrial Case Study, Ind. Eng. Chem. Res. 45 (2006) 2994-3000.

[11] J. Shu, B.P.A. Grandjean, S. Kaliaguine, Methane steam reforming in asymmetric Pd- and Pd-Ag/porous SS membrane reactor, Appl. Catal., A 119 (1994) 305-325.

[12] I. Yasuda, Y. Shirasaki, Development and Demonstration of Membrane Reformer System for Highly-efficient Hydrogen Production from Natural Gas, Mater. Sci. Forum 539-543 (2007) 1403-1408.

[13] Y. Shirasaki, T. Tsuneki, Y. Ota, I. Yasuda, S. Tachibana, H. Nakajima, K. Kobayashi, Development of membrane reformer system for highly efficient hydrogen production from natural gas, Int. J. Hydrogen Energy 34 (2009) 4482-4487.

[14] H. Kurokawa, Y. Shirasaki, I. Yasuda, Energy-Efficient Distributed Carbon Capture in Hydrogen Production from Natural Gas, Energy Procedia 4 (2011) 674-680.

[15] T.L. Ward, T. Dao, Model of hydrogen permeation behavior in palladium membranes, J. Membr. Sci. 153 (1999) 211-231.

[16] B.D. Morreale, M.V. Ciocco, R.M. Enick, B.I. Morsi, B.H. Howard, A.V. Cugini, K.S. Rothenberger, The permeability of hydrogen in bulk palladium at elevated temperatures and pressures, J. Membr. Sci. 212 (2003) 87-97.

[17] A.L. Mejdell, M. Jøndahl, T.A. Peters, R. Bredesen, H.J. Venvik, Experimental investigation of a microchannel membrane configuration with a 1.4 μm Pd/Ag23wt.% membrane – Effects of flow and pressure, J. Membr. Sci. 327 (2009) 6-10.

[18] L.S. McLeod, F.L. Degertekin, A.G. Federov, Determination of the rate-limiting mechanism for permeation of hydrogen through microfabricated palladium-silver alloy membranes, J. Membr. Sci. 341 (2009) 225-232.

[19] R. Dittmeyer, V. Höllein, K. Daub, Membrane reactors for hydrogenation and dehydrogenation processes based on supported palladium, J. Mol. Catal. A: Chem. 173 (2001) 135-184.

[20] H. Amandusson, L.-G. Ekedahl, H. Dannetun, The effect of CO and O_2 on hydrogen permeation through a palladium membrane, Appl. Surf. Sci. 153 (2000) 259-267.

[21] A.L. Mejdell, M. Jøndahl, T.A. Peters, R. Bredesen, H.J. Venvik, Effects of CO and CO_2 on hydrogen permeation through a ~3 μm Pd/Ag 23 wt.% membrane employed in a microchannel membrane configuration, Sep. Purif. Technol. 68 (2009) 178-184.

[22] A.L. Mejdell, D. Chen, T.A. Peters, R. Bredesen, H.J. Venvik, The effect of heat treatment in air on CO inhibition of a ~3 μm Pd-Ag (23 wt.%) membrane, J. Membr. Sci. 350 (2010) 374-377.

[23] S. Hara, K. Sakaki, N. Itoh, Decline in Hydrogen Permeation Due to Concentration Polarization and CO Hindrance in a Palladium Membrane Reactor, Ind. Eng. Chem. Res. 38 (1999) 4913 – 4918

[24] N. Mori, T. Nakamura, K. Noda, O. Sakai, A. Takahashi, N. Ogawa, H. Sakai, Reactor Configuration and Concentration Polarization in Methane Steam Reforming by a Membrane Reactor with a Highly Hydrogen-Permeable Membrane, Ind. Eng. Chem. Res. 46 (2007) 1952-1958.

[25] A. Caravella, G. Barbieri, E. Drioli, Concentration polarization analysis in self-supported Pd-based membranes, Sep. Purif. Technol. 66 (2009) 613-624.

[26] S.-K. Ryi, J.-S.Park, K.-R.Hwang, C.-B.Lee, S.-W. Lee, Module configuration in CO_2 capture using Pd-based composite membranes, Int. J. Hydrogen Energy 36 (2011) 13769-13755.

[27] K.-R. Hwang, S.-K.Ryi, C.-B.Lee, S.W. Lee, J.-S. Park, Simplified, plate-type Pd membrane module for hydrogen purification, Int. J. Hydrogen Energy 36 (2011) 10136 – 10140.

[28] A.Y. Tonkovich, S. Perry, Y. Wang, D. Qiu, T. LaPlante, W.A. Rogers, Microchannel process technology for compact methane steam reforming, Chem. Eng. J. 59 (2004) 4819 – 4824.

[29] R. Bredesen and H. Klette, Method of manufacturing thin metal membranes, US Patent 6,086,729.

[30] T.A. Peters, M. Stange, R. Bredesen, On the high pressure performance of thin supported Pd-23%Ag membranes – Evidence of ultrahigh hydrogen flux after air treatment, J. Membr. Sci. 378 (2011) 28-34.

[31] A.L. Mejdell, H. Klette, A. Ramachandran, A. Borg, R. Bredesen ,Hydrogen permeation oft thin, free-standing Pd/Ag23% membranes before and after heat treatment in air, J. Membr. Sci. 307 (2008) 96-104.

[32] W.M. Tucho, H.J. Venvik, J.C. Walmsley, M. Stange, A. Ramachandran, R.H. Mathiesen, A. Borg, R. Bredesen, R. Holmenstad, Microstructural studies of self-supported (1.5-10 μm) Pd/23 wt%Ag hydrogen separation membranes subjected to different heat treatments, J. Mater. Sci. 44 (2009) 4429-4442.

[33] G. Zeng, A. Goldbach, H. Xu, Impact on mass flow resistance on low-temperature H_2 permeation characterisitcs of a $Pd_{95}Ag_5/Al_2O_3$ composite membrane, J. Membr. Sci. 326 (2009) 681-687.

[34] J. Okazaki, D.A. Pacheco Tanaka, M.A. Llosa Tanco, Y. Wakui, F. Mizukami, T.M. Suzuki, Hydrogen permeability study of the thin Pd-Ag alloy membranes in the temperature range across the α-β phase transition, J. Membr. Sci. 282 (2006) 370-374.

[35] S.N. Paglieri, J.D. Way, Innovations in Palladium Membrane Research, Sep. Purif. Technol. Reviews 31 (2002) 1-169

[36] P.P. Mardilovich, Y. She, Y.H. Ma, Defect-Free Palladium Membranes on Porous Stainless-Steel Support, AIChE J. 44 (1998) 310-322.

[37] H. Amandusson, L.-G. Ekedahl, H. Dannetun, Hydrogen permeation through surface modified Pd and PdAg membranes, J. Membr. Sci. 193 (2001) 35-47.

[38] L. Shi, A. Goldbach, G. Zeng, H. Xu, Direct synthesis over Pd membranes at elevated temperatures, J. Membr. Sci. 348 (2010) 160-166.

[39] X.L. Pan, N. Stroh, H. Brunner, G.X. Xiong, S.S. Sheng, Pd/ceramic hollow fibers for H_2 separation, Sep. Purif. Technol. 32 (2003) 265-270.

[40] X.L. Pan, G.X. Xiong, S.S. Sheng, N. Stroh, H. Brunner, Thin dense Pd membranes supported on α-Al_2O_2 hollow fibers, Chem. Commun. (2001) 2536-2537.

[41] F. Roa, M.J. Block, J.D. Way, The influence of alloy composition on the H_2 flux of composite Pd-Cu membranes, Desalination 147 (2002) 411-416.

[42] F. Roa and J.D. Way, Influence of Alloy Composition and Membrane Fabrication on the Pressure Dependence of the Hydrogen Flux of Palladium-Copper Membranes, Ind. Eng. Chem. Res. 42 (2003) 5827-5835.

[43] L. Bortolotto, R. Dittmeyer, Direct hydroxylation of benzene to phenol in a novel microstructured membrane reactor with distributed dosing of hydrogen and oxygen, Sep. Purif. Technol. 73 (2010) 51-58.

[44] X.L. Pan, M. Kilgus, A. Goldbach "Low-temperature H_2 and N_2 transport through thin $Pd_{66}Cu_{34}H_x$ layers" Catal. Today 104 (2005) 225-230.

[45] J. Chabot, J. Lecomte, C. Grumet, J. Sannier, Fuel Clean-Up System: Poisoning of Palladium-Silver Membranes by Gaseous Impurities, Fusion Technology 14 (1988) 614-618.

[46] E. Serra, M. Kemali, A. Perujo, D.K. Ross, Hydrogen and Deuterium in Pd-25 Pct Ag Alloy: Permeation, Diffusion, Solubilization, and Surface Reaction, Metall. Mater. Trans. A 29A (1998) 1023-1028.

[47] F. Scura, G. Barbieri, E. Drioli "H_2 for PEM-FC: effect of CO in the purification by means of Pd-based membranes" Desalination 200 (2006) 239-241.

Figure 1: Microstructured foils with a Pd-based membrane arranged between the sheets.

Figure 2: Laser-welded membrane module.

Figure 3: Housing for the membrane module with connections for gas supply.

Figure 4: Schematic of the microstructured module with integrated palladium-based membrane.

Figure 5: Tentative partial pressure profile from the retentate side (R) across the membrane to the permeate side (P) and the anticipated boundary layer resembling the mass transfer resistance from the bulk gas phase to the membrane surface.

Figure 6: Film effectiveness factor η as a function of ϕ with ρ as a parameter.

Figure 7: SEM pictures of the fresh membranes surfaces: a) PdCu, b) Pd c) PdAg (13 µm) and d) PdAg (4.7 µm).

Figure 8: Cross-sections of the membrane modules with the integrated a) 61µm PdCu membrane, b) 13 µm PdAg membrane and c) 4.7 µm PdAg membrane.

Figure 9: Hydrogen flux at 350°C as a function of the difference of the square root of the hydrogen partial pressure for the four Pd-based membranes tested.

Figure 10: Arrhenius plot of the four analyzed Pd-based membranes.

Figure 11: Experimental and calculated H_2 flux for mixed gas experiments as a function of total feed flow; Experimental conditions: p_{Ret} =300 kPa, 50% H_2 in N_2, PdAg membrane: T = 300°C, Pd membrane: 350°C.

Figure 12: Calculated film effectiveness factor η_{glob} and H_2 recovery factor φ_{H2} as a function of total feed flow; Conditions as in Fig. 12.

Figure 13: Film effectiveness factor η and H_2 flux as a function of channel length for the 4.7 µm PdAg membrane at 300 kPa and a feed flow rate of 400 ml/min.

Figure 14: Film effectiveness factor η and H_2 flux as a function of channel length for the 4.7 µm PdAg membrane at 300 kPa and a feed flow rate of 60 ml/min.

Table 1: Thickness, WDX analysis (at.%), experimental conditions and ideal

Material	s [µm]	Composition Front PdX [%/%]	Composition Back PdX [%/%]	T [°C]	p_{Ret} [kPa]	S
PdCu	61.0	47.15/52.85	-/-	350 - 400	150 – 650	> 1
Pd	12.5	-/-	-/-	350 - 400	150 – 450	> 30
PdAg	13.0	80.02/19.98	80.03/19.97	300 - 350	150 – 450	> 20
PdAg	4.7	80.58/19.42	80.38/19.62	300 - 350	50 - 300	> 4

permselectivities of the tested membrane modules.

Table 2: Comparison of experimental values with literature data in the specific temperature and pressure range; $p_{H2,Perm}$ = 101.3 kPa if permeate side was atmospheric pressure and no other stated in the paper.

ort	s [µm]	$p_{H2,Ret}$ [kPa]	$p_{H2,Perm}$ [kPa]	T [°C]	Q_0 [10^{-7} mol/msPa$^{0.5}$]	E_a [kJ/mol]	$Q_{T=350°C}$ [10^{-8}mol/msPa$^{0.5}$]	S [-]
	1000	91 – 275.7	Ar sweep	350 - 900	1.92	13.8	1.34	∞
	19-28	100 - 600	101.3	350 - 700	n.a.	16.4	n.a.	n.a.
	25	0.133 – 3.325	Ar sweep	100 - 350	n.a.	11.0	n.a.	n.a.
	0.5	200	101.3	350 - 500	1.49E-01	9.7	2.29E-01	846 - 1359
	0.5	200	101.3	350 - 500	3.63E-01	10.3	4.97E-01	1132 - 2185
	2 - 3	115 - 265	98.5	350 - 450	n.a.	14.6	n.a.	~1000
	2-3	190	101.3	335 - 400	n.a.	15.8	n.a.	> 1000
	12.5	250 - 450	101.3	350 - 400	2.59	14.6	1.56	> 30.000
	1	510	83	350	n.a.	n.a.	1.29E-01	1390
	1.5	273	83	350	n.a.	n.a.	5.79E-01	93
	50	100 - 300	N2 sweep	150 - 180	4.54E-02	16.1	n.a.	∞
SS	5	100 - 300	N2 sweep	150 - 180	n.a.	4.0 – 4.7	n.a.	n.a.
F	4	500	98.5	25 - 510	5.87E-01	21.3	9.61E-02	> 2000
	61.0	250 - 650	101.3	350 - 400	6.34E-01	6.5	1.80	> 1900
C	~1	4.5 – 36.4	Ar sweep	250 - 450	5.10E-01	10.8	6.34E-01	n.a.
	2	100 - 200	101.3	187 - 550	2.44E-01	9.0	4.30E-01	> 4700
	25	0.133 – 3.325	Ar sweep	100 - 350	n.a.	6.0	n.a.	n.a.
	250	14	vacuum	100 - 450	4.95E-01	5.9	1.60	n.a.
	198 - 782	0.001 - 100	vacuum	25 - 300	5.58E-01	6.3	1.72	n.a.
	60	200 - 700	100	374 - 429	9.7	25.8	6.72E-01	n.a.
	13.0	250 - 450	101.3	300 - 350	3.14	11.3	3.57	> 20.000
	4.7	150 - 300	101.3	300 - 350	1.91	10.4	2.55	>4250

CHF = Ceramic hollow fibre; CR = Cold-rolled; ELP = electroless plating; MC = Microchannel; MS = Magnetron Sputtering; PC = Porous ceramic; PECVD = Plasma enhanced chemical vapour deposition; PM = Preparation method; PSS = porous stainless steel